Electrochimica Acta 462 (2023) 142739

Contents lists available at ScienceDirect

Electrochimica Acta

journal homepage: www.journals.elsevier.com/electrochimica-acta

Reversible heat effects of lithium metal- and porous lithium iron phosphate electrodes

Astrid Fagertun Gunnarshaug [a], Odne Stokke Burheim [b,*], Signe Kjelstrup [a]

[a] PoreLab, Department of Chemistry, Norwegian University of Science and Technology, NTNU, Trondheim, Norway
[b] Department of Energy and Process Engineering, Norwegian University of Science and Technology, NTNU, Trondheim, Norway

ARTICLE INFO

Keywords:
Reversible heat
Peltier heat
Seebeck coefficient
Reaction entropy $LiFePO_4$

ABSTRACT

We report Peltier heats and reaction entropy of cells with lithium metal- and near fully lithiated lithium iron phosphate (LFP) electrodes. The Peltier heats were measured through the Seebeck coefficient of thermogalvanic cells. The value obtained for the Peltier heat of Li-metal, −32 ± 3 kJ/mol at 298 K, supports previously reported values. When close to being fully lithiated, LFP goes through a phase transition from a two-phase mixture to a solid solution. The value of Peltier heats obtained for LFP vary from −15 ± 1 to −72 ± 9 kJ/mol. The variation is explained by large entropy changes of lithium iron phosphate, near the phase transition. The cell entropy difference of lithium iron phosphate against lithium metal varied from −64 ± 3 to +50 ± 20 J/K mol. The negative Peltier heats means that the electrodes generates heat when acting as an anode, which leads to a temperature rise in the electrode compartment, and absorbs heat when acting as a cathode. The local reversible heat effect is equal to or larger in magnitude than the net reversible heat effect. The time-dependence of the Seebeck coefficient, the Soret effect, was found to differ between the cells with planar Li-metal electrodes to porous LFP.

1. Introduction

Lithium ion batteries have become one of the key energy storage technologies for the transition towards renewable energy sources. The performance and degradation of lithium-ion batteries has been linked to thermal effects [1]. To understand ageing processes and improve thermal management, we need to know possible thermal profiles at a cell level. For this we need detailed knowledge of thermal properties and local sources and sinks of heat in the cell.

Heat generation in batteries consists of irreversible- and reversible heat effects. Irreversible heat is generated due to internal losses in the battery, and leads to a temperature rise independent of the direction of the current, while the reversible heat effect changes sign upon on a change of the direction of the current [2]. This can lead to a net cooling effect in the battery [3].

Reversible heat effects are usually studied through the reaction entropy of the cell, measured through the temperature dependence of the cell's emf (potentiometric method), often using lithium metal as a reference electrode [4]. The reaction entropy gives information of the net reversible heat generated in the battery. Recently, the single electrode reversible heat effect has received more attention [5–8]. During the (reversible) electrode reaction, heat is produced or absorbed at the electrode surface [9,10]. This reversible heat effect is the Peltier heat [11]. The Peltier heat may cause the electrode to either cool or heat, depending on the direction of the current.

The Peltier heat of an electrode–electrolyte surface is defined as the reversible heat needed to keep the temperature constant when one faraday of positive charges passes from the electrode to the electrolyte [11]. The Peltier heats of the electrodes in a battery can be subtracted from left to right under isothermal conditions and sufficiently similar electrolyte conditions, to give the reaction entropy change of the cell times the cell temperature [12,13]:

$$T\Delta S = \Pi^a - \Pi^c \tag{1}$$

This is an entropy balance of the electrode surfaces under reversible conditions. Here T is the cell temperature, ΔS is the cell entropy change due to the electrode reactions, and Π^a and Π^c refer to the anode and cathode Peltier heats respectively, as measured from the Seebeck coefficient [14] (see below). They have also been referred to as single electrode entropies [5] and single electrode temperature coefficients [6].

Eq. (1) has been used to calculate the Peltier heat of individual electrodes from reaction entropies [6,14–16]. Behind Eq. (1) there is an assumption of isothermal conditions and constant composition and a current density $j \approx 0$. The surroundings of the electrolyte adjacent

* Corresponding author.
E-mail addresses: odne.s.burheim@ntnu.no (O.S. Burheim), signe.kjelstrup@ntnu.no (S. Kjelstrup).

https://doi.org/10.1016/j.electacta.2023.142739
Received 12 May 2023; Received in revised form 7 June 2023; Accepted 12 June 2023
Available online 14 June 2023

to the two electrode surfaces must be the same. To the best of our knowledge, the validity of the assumptions behind Eq. (1) has not been discussed for LIB electrodes. We will return to this in Section 2.3.

The electrolyte contributes to the local heat effects at the surface, by adding terms on one side and subtracting on the other. However, the two contributions cancel in Eq. (1). The single electrode Peltier heat has contributions from the electrolyte. Therefore, in order to consider local electrolyte contributions in thermal models, we need the single electrode Peltier heats of the battery.

Lithium iron phosphate is one of the electrode materials commonly used in commercial batteries [17]. It has low cost [18] and low environmental impact [19]. Lithium metal electrodes are much used in battery research, and measurement of reversible heat generation is often done with a lithium metal anode [1]. In this work we take a closer look at the single electrode Peltier heats and reaction entropies of the Li ‖ $LiFePO_4$ cell.

1.1. State of the art

1.1.1. Cell entropy of Li ‖ $LiFePO_4$

The reaction entropy change in Eq. (1) is related to the temperature dependence of the cell's emf:

$$\Delta S = nF\frac{\partial\left(\Delta\phi\right)_{j=0}}{\partial T} \tag{2}$$

where $\Delta\phi_{j=0}$ is the emf of the cell.

Few reaction entropies have been reported for the cell Li ‖ $Li_{1-x}FePO_4$ [3,6,15,20], and fewer still with detailed entropy data for $x \to 0$ and $x \to 1$. The data available suggests that Li ‖ $Li_{1-x}FePO_4$ has small entropy changes with small variations of ± 10 J/K mol [3,4], except when the compound is close to fully lithiated or de-lithiated. LFP goes through a phase transition to a single-phase solid solution when $x \to 0$ or $x \to 1$ [21]. The solid solution is promoted at elevated temperatures — the transition is an entropy driven process [22], which depends on the particle size of LFP [23]. The stable reaction entropy for intermediate lithiated states is explained by LFP existing as a two-phase mix at intermediate lithiated states.

Yamada and co-workers measured the heat flow of a Li ‖ $Li_{1-x}FePO_4$ cell under a C/20 discharge [21], and saw a large variation in the heat flow near full lithiation of LFP, and a stable heat flow in the intermediate regions. From their data we can estimate a change in ΔS from roughly −30 J/K mol to 35 J/K mol to roughly 15 J/K mol between lithiated states of $x \approx 0$ and $x \approx 0.11$. We note that measurements of heat flow in a cell will have a contribution from irreversible heat evolution, even at low currents.

1.1.2. Peltier heats of Li and $LiFePO_4$

Peltier heats can be measured directly [24], but are usually found through the Seebeck coefficient of a thermogalvanic cell [25]. The Peltier and Seebeck effects are reciprocal effects, related through the Onsager relations [11]. Each Peltier heat in Eq. (1) can be computed from Seebeck coefficients of thermogalvanic cells with two identical electrodes, of materials a or c, respectively, in the absence of composition gradients:

$$\left[\Pi\right]_{dT=0,d\mu_T=0}/T = -\left(\frac{\Delta\phi}{\Delta T}\right)_{j=0,d\mu_T=0} \tag{3}$$

Here T is the mean temperature of the thermogalvanic cell and μ_T is the chemical potential evaluated at temperature T. The subscript $d\mu_T = 0$ refers to uniform electrolyte composition at this temperature. The Peltier heat measured through the Seebeck coefficient refers to that of an anode reaction. The Peltier heat has the same value, but opposite sign ($-\Pi$) when acting as a cathode. This is why Π^c is subtracted in Eq. (1); the value of Π^c refers to the measured value from the Seebeck coefficients, which corresponds to the anodic electrode reaction.

Seebeck coefficients are measured through the response in the emf of a thermogalvanic cell when a temperature difference is applied across the electrolyte. Due to coupling of mass- and heat transfer, a phenomena known as the Soret effect, concentration gradients will develop in the electrolyte during the experiment. Concentration gradients will contribute to the emf of the thermogalvanic cell. The right-hand side of Eq. (3) corresponds to the Seebeck coefficient prior to the establishment of concentration gradients. At $t = 0$, $\eta_0 = (\Delta\phi/\Delta T)_{j=0,d\mu_T=0}$. At stationary state a balance is reached between the chemical- and thermal forces, and we define $\eta_\infty = (\Delta\phi/\Delta T)_{j=0,t=\infty}$.

The first Seebeck coefficient of LIB thermogalvanic cells were, to the best of our knowledge, reported by Kuzminskii et al. in 1993 [26]. Several groups have reported η_0 more recently [5,16,25,27,28]. The Seebeck coefficient has been referred to as a "temperature coefficient" of single electrode potentials [6,7,15]. We refer to [6,14,29] for overviews of Peltier heat measurements for LIBs.

The Seebeck coefficient of lithium-metal thermogalvanic cells are of special interest, since many ΔS are reported with Li-metal as an anode. This allows us to compute the Peltier heat of the Li-metal electrode surface. From there we can use Eq. (1) and ΔS measurements to compute the Peltier heat of other electrodes. Seebeck coefficients of Li-metal thermogalvanic cells have been reported by several groups [7, 15,16,27,28]; there seems to be a consensus for a value of around 1 mV/K, depending on the electrolyte. This corresponds to a Peltier heat of around −30 kJ/mol for the Li-metal surface. To the best of our knowledge, no group has reported the Soret effect in these experiments.

We know of only two reports for lithium iron phosphate (LFP). Our group found a remarkably high Seebeck coefficient of 3.7 ± 0.8 mV/K at stationary state, with an initial value of 1.3 ± 0.4 mV/K. The electrolyte was 1 M $LiPF_6$ in 1:1 w% ethylene carbonate (EC): diethyl carbonate (DEC) and the cell was assembled as a pouch. Swiderska et al. reported a value of 0.86 mV/K [6] in a LFP thermogalvanic cell with a 1 M $LiPF_6$ in ethylene carbonate (EC)/dimethyl carbonate (DMC) electrolyte. Due to the experimental set-up, with electrodes far apart and a vertical electrode arrangement, we suspect that the value is the Seebeck coefficient of the electrolyte at uniform composition.

While both measurements were performed close to full lithiation, our measured Seebeck coefficient at initial times (1.3 mV/K) were roughly 50% larger than that reported by Swiderska et al. (0.86 mV/K). As already mentioned, LFP near full lithiation is known to go through a phase transition. Large reaction entropy variations caused by the phase transition give us reason to suspect that also the Peltier heat of LFP may also vary significantly.

1.2. The objective

The objective of this work is to report Seebeck coefficients/Peltier heats of Li-metal and commercial $LiFePO_4$ (LFP) thermogalvanic cells at initial and stationary state, and the reaction entropy differences of the Li ‖ LFP battery when LFP is close to fully lithiated. These data are needed for modelling purposes [30]. We shall see that the values for the Li-metal thermogalvanic cell support previous reports. In addition we shall see that the values of LFP vary significantly, closely mirrored by large variations in the reaction entropy of Li ‖ LFP.

In this article, we report new data, while we at the same time take a closer look into the conditions behind Eq. (1). We suspect that deviations from Eq. (1) may occur, when one or both electrodes are porous. In that case, we can no longer expect that transport properties of the electrolyte in the electrode compartment are the same as for the bulk. A consistency check of Eq. (1) can be performed, when both single Peltier heats as well as the cell entropy changes are measured. The results will have impact on how single electrode reversible heat effects are measured and reported or modelled.

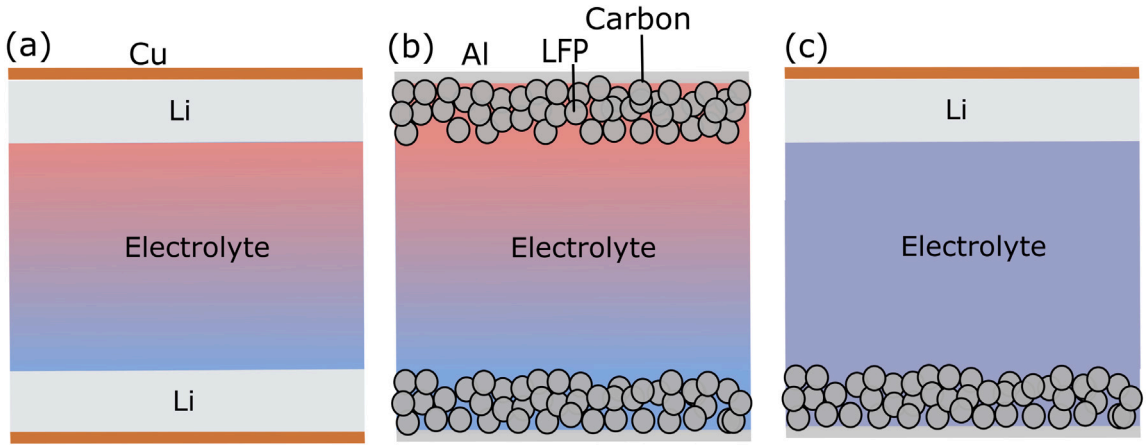

Fig. 1. Schematic of cells studied. (a) non-isothermal symmetric Li-cell (thermogalvanic cell), (b) non-isothermal symmetric LFP-cell (thermogalvanic cell), and (c) isothermal Li || LFP cell.

2. Theory

2.1. Cell descriptions and electrode reactions

An isothermal Li || LFP cell is used in this work to measure the reaction entropy (see Fig. 1(c)). It consists of a Li-metal negative electrode with a copper lead, a $LiPF_6$ in 1:1 ethylene carbonate (EC): diethyl carbonate (DEC) electrolyte and a $LiFePO_4$ positive electrode. LFP consist of many small particles with a carbon coating on an aluminium backing.

$$\mathrm{Cu(s)|Li(s)|\ electrolyte\ |LiFePO_4(s)|C(s)|Al(s)}$$

The reaction of LFP depends on the state it is in. For lithiated states $\alpha > x > \beta$, where α and β depends on particle size [23] and temperature [20], LFP exists in a two-phase mixture of $LiFePO_4$ and $FePO_4$. Outside of these regions, LFP is a single phase material with lithium statistically distributed within the electrode particles, cf. Fig. 2. Hence, the two possible electrode reactions for the Li || LFP cell are:

$$\mathrm{Li(s)} + \frac{1}{\Delta x}\mathrm{Li_{1-(x+\Delta x)}FePO_4(s)} \rightleftharpoons \frac{1}{\Delta x}\mathrm{Li_{1-x}FePO_4(s)}$$
$$\mathrm{Li(s)} + \mathrm{FePO_4(s)} \rightleftharpoons \mathrm{LiFePO_4(s)}$$

and the half-cell reactions:

$$\mathrm{Li(s)} \rightleftharpoons \mathrm{Li^+(non-aq)} + \mathrm{e^-(s)}$$
$$\frac{1}{\Delta x}\mathrm{Li_{1-x}FePO_4(s)} \rightleftharpoons \mathrm{Li^+(non-aq)} + \mathrm{e^-(s)} + \frac{1}{\Delta x}\mathrm{Li_{1-(x+\Delta x)}FePO_4(s)}$$
$$\mathrm{LiFePO_4(s)} \rightleftharpoons \mathrm{Li + (non-aq) + e^-(s) + FePO_4(s)}$$

We write the reaction entropy as:

$$\Delta S = \Delta S^{\mathrm{LFP}} - S_{\mathrm{Li}} \tag{4}$$

where ΔS^{LFP} is the entropy change of LFP due to intercalation of lithium. From the half-cell reactions we find two possible entropies of lithiation:

$$\Delta S^{\mathrm{LFP}} = \begin{cases} \frac{1}{\Delta x} S_{\mathrm{Li_{1-(x+\Delta x)}FePO_4(s)}} - \frac{1}{\Delta x} S_{\mathrm{Li_{1-x}FePO_4}}, & x < \beta, x > \alpha \\ S_{\mathrm{LiFePO_4}} - S_{\mathrm{FePO_4(s)}}, & \alpha > x > \beta \end{cases} \tag{5}$$

In this work we use commercial LFP close to full lithiation. The value of x determines whether we have a two-phase material or a solid solution.

The charging-curve of Li || LFP cell is shown in Fig. 2. As is typical behaviour of LFP [31], in the region around $x = 0$ we find a steep increase in the potential with decreasing lithium concentration. The cell then reaches a stable region where the potential is invariant to changes in lithium concentration of LFP; this is the two-phase region [32]. Towards the end of the charging, the potential increases rapidly. We label the regions with changing potential as single-phase regions [32].

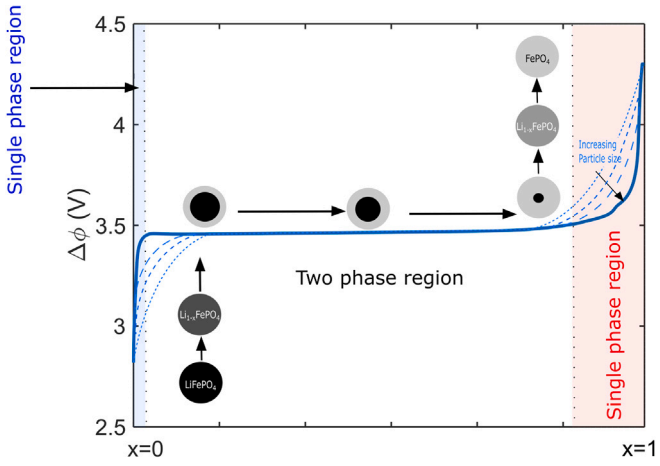

Fig. 2. Voltage charge-curve for the Li || LFP cell where a charging current of 0.127 mA was used. An illustration of the phase-transition and shrinking-core model for lithium-insertion into LFP is added [31–34]. The blue and red-shades are added to highlight the single-phase regions. The particle-size has an impact for the shape of the voltage curve. The stippled line are added to indicate the effect of changing particle size, and is meant as a qualitative illustration only. The electrodes in this study were commercial electrodes with a particle size in the μmeter range.

2.2. Thermogalvanic cell description and theory

We present the equations that describe the Seebeck coefficient of a thermogalvanic cell, needed to calculate the Peltier heat of an electrode surface. For a detailed theoretical description of Li-ion thermoelectric cells, we refer to earlier work [14,25], but a summary of the most important equations can be found below.

We determine the Seebeck coefficients of following (symmetric) Li-metal and LFP thermogalvanic cells (see Fig. 1(a) and (b)), with a $LiPF_6$ in 1:1 ethylene carbonate (EC): dimethyl carbonate (DMC) electrolytes:

$$\mathrm{Cu(s)|Li(s,}T_1\mathrm{)|\ electrolyte\ |Li(s,}T_2\mathrm{)|Cu(s)}$$
$$\mathrm{Al(s)|C(s)|Li_{1-x}FePO_4(s,}T_1\mathrm{)|\ electrolyte\ |Li_{1-x}FePO_4(s,}T_2\mathrm{)|C(s)|Al(s)}$$

The thermogalvanic cells are kept at the same average temperature $(T_1 + T_2)/2$.

The Peltier heat is the reversible heat effect at an electrode surface. Following Gibbs' definition of the dividing surface, the electrode surface is treated as a discontinuity between the electrode and electrolyte bulk phases. The surface is treated as its own thermodynamic system [11].

The thermogalvanic cell theory describes the Seebeck coefficient as an emf measurement between two identical electrode surfaces (symmetric electrode arrangement) at different temperatures [25]. The Peltier heat measured through the Seebeck coefficient is the Peltier heat for an oxidation reaction [10,12,14]. It follows from the Onsager relations that a positive Seebeck coefficient gives a negative Peltier heat [35]. A negative Peltier heat means that heat is released to the surroundings. Reversible heat must be removed to keep the surfaces isothermal.

The Peltier heat is obtained from an entropy balance at the electrode at the start of the experiment [12]. Entropy is liberated or consumed by the electrode reaction, transported with electrons in the electrode/current collectors and transported away from the electrode surface by the charged components in the electrolyte. In addition we must include the entropy liberated due to removal of neutral components following the electric current in the entropy balance. We obtain:

$$\frac{\Pi^a}{T} = -S_{\mathrm{Li}} + S^*_{\mathrm{e^-}} + \left(t_{\mathrm{Li^+}} S^*_{\mathrm{Li^+}} - t_{\mathrm{PF_6^-}} S^*_{\mathrm{PF_6^-}}\right) + t_{\mathrm{LiPF_6}} S_{\mathrm{LiPF_6}} + t_{\mathrm{DEC}} S_{\mathrm{DEC}} \quad (6)$$

Here S_i^* is the transported entropy of component i, and t_i is the transference coefficient or transport number of component i. The nth component in the last sum is not included; it is used as the frame of reference. We see that the electrolyte's contribution to the Peltier heat, is related to the transport properties and state of the electrolyte *adjacent* to the electrode surface, what we call the electrode compartment. The third term on the right-hand side is related to entropy changes due to charge transport. The last two terms on the right-hand side give the entropy liberated when neutral electrolyte components are transported away from the surface.

Following equation Eq. (3), we find the Seebeck coefficient of Li-metal at uniform electrolyte composition with n electrolyte components [11,14,25]:

$$\eta_0 = \frac{1}{F}\left(S_{\mathrm{Li}} - S^*_{\mathrm{e^-}} - \left(t_{\mathrm{Li^+}} S^*_{\mathrm{Li^+}} - t_{\mathrm{PF_6^-}} S^*_{\mathrm{PF_6^-}}\right) - \sum_{i=1}^{n-1} t_i S_i\right) \quad (7)$$

When a balance has been reached between the thermal and chemical forces (at $t = \infty$), and a Soret equilibrium has been established, there is no net mass flux of neutral components and no net transport of anions. Therefore, we are left with only entropy transported by the single charge carrier (lithium ions) and entropy liberated in the electrode reaction. We are left with the following expression for the Seebeck coefficient at stationary state (η_∞):

$$\eta_\infty = \left(\frac{\Delta\phi}{\Delta T}\right)_{j=0,t=\infty} = \frac{1}{F}\left(S_{\mathrm{Li}} - S^*_{\mathrm{e^-}} - S^*_{\mathrm{Li^+}}\right) \quad (8)$$

The Seebeck coefficient of LFP thermogalvanic cells are obtained in the same manner. The expression will depend on the phase which determines the electrode reaction. We take the two phase reaction as an example. During the oxidation reaction, one mole of $LiFePO_4$ is consumed, and $S_{\mathrm{LiFePO_4}}$ is liberated, while one mole of $FePO_4$ is liberated, consuming $S_{\mathrm{FePO_4}}$. We find:

$$\Pi^{\mathrm{c}} = T\left(-\Delta S^{\mathrm{LFP}} + S^{*\mathrm{c}}_{e^-} + \left(t_{\mathrm{Li^+}} S^*_{\mathrm{Li^+}} - t_{\mathrm{PF_6^-}} S^*_{\mathrm{PF_6^-}}\right) + \sum_{i=1}^{n-1} t_i S_i\right) \quad (9)$$

2.3. Remark on Peltier heats and the reaction entropy of batteries

We can now take a closer look at Eq. (1). When subtracting the two Peltier heats of a battery, we see that:

$$\begin{aligned}\Pi^a - \Pi^c = & T^{\mathrm{a}}\left(-\Delta S^{\mathrm{a}} + S^{*\mathrm{a}}_{e^-} + t^{\mathrm{a}}_{\mathrm{Li^+}} S^{*,\mathrm{a}}_{\mathrm{Li^+}} - t^{\mathrm{a}}_{\mathrm{PF_6^-}} S^{*,\mathrm{a}}_{\mathrm{PF_6^-}} + \sum_{i=1}^{n-1} t^{\mathrm{a}}_i S_i\right) - \\ & T^{\mathrm{c}}\left(-\Delta S^{\mathrm{c}} + S^{*\mathrm{c}}_{e^-} + t^{\mathrm{c}}_{\mathrm{Li^+}} S^{*,\mathrm{c}}_{\mathrm{Li^+}} - t^{\mathrm{c}}_{\mathrm{PF_6^-}} S^{*,\mathrm{c}}_{\mathrm{PF_6^-}} + \sum_{i=1}^{n-1} t^{\mathrm{c}}_i S_i\right)\end{aligned} \quad (10)$$

Under the assumption of isothermal conditions, $T^{\mathrm{a}} = T^{\mathrm{c}}$, and that the transport properties in the electrolyte do not change, Eq. (10) reduces to Eq. (1). When there is a temperature gradient across the battery, we are no longer at equilibrium conditions. For now we neglect the temperature dependence of the transport properties.

The S_i^* and t_i are weakly composition-dependent properties, but will differ between the surface and bulk. For porous electrodes, they may also differ between the electrolyte within the electrode pores and the bulk solution.

3. Materials and methods

3.1. Cell assembly

All cells were assembled as pouch-cells in an argon filled glove box. The thermogalvanic cells had a symmetric electrode arrangement. The electrode material was either lithium-chips from TMAX (0.25 mm thick) or electrode sheets of carbon coated $LiFePO_4$ (HS-LIB-P-LFP-001, 70 μm electrode material, 30 μm Al backing) from Hohsen. For the reaction entropy measurements, cells were assembled with one $LiFePO_4$ and one lithium-metal electrode, where the $LiFePO_4$ electrodes were extracted from LFP thermogalvanic cells made with 20 and 80 s vacuum sealing time (see Table 2). Copper and aluminium foil was used as tabs for the Li-metal and LFP electrodes, respectively. The electrodes were pristine. A stack of 4 Whatman Glass Microfibre Filters GF/D (no 1823070, pore diameter of 2.7 μm) were used as a separator for the thermogalvanic cell, while only one was used for the isothermal cell. The stack was sandwiched between the two electrodes, and had a thickness of 1.8 mm after vacuum sealing. The electrolytes were 1 M $LiPF_6$ in 1:1 v/v EC/DMC from Sigma Aldrich. The voltage-curve was recorded for a Li ‖ $LiFePO_4$ cell with the same electrodes, but with an LP40 electrolyte (1 M $LiPF_6$ in a 1:1 weight% EC/DEC) from Gotion. The PC8 pouch-cell laminate from Targray was used, and a polypropylene film was used to reinforce the seal around the tabs. Electrolyte was added to the separators until the separators were soaked, but not dripping, approximately 1 mL per cell.

The stack thickness was chosen to maintain a thermal gradient across the cell, while still keeping the characteristic time for diffusion in the electrolyte low enough to allow the Soret effect to be observed within a reasonable time-frame. The characteristic time is given as $\theta = l^2/\pi^2 D$, where l is the diffusion path length and D is the diffusion coefficient. Assuming a diffusion coefficient of 1–3 $\times 10^{-10}$ m^2/s [36–38] gives a characteristic time between 18 and 55 min, in bulk electrolyte.

The pouch cells were sealed with an Audion VMS 53 Vacuum Chamber. Vacuum was applied followed by heat-sealing of the last edge of the pouch (4 s). The lowest pressure was reached after 15 s. We report results for sealing times of thermogalvanic cells as $x + 4$, where x is the time spent under lower pressure before heat was applied (from 4 to 99 s). For sealing times less than 15 s, the lowest pressure was never reached. For sealing times longer than 15 s, the remaining time was spent under vacuum. For Li ‖ LFP cells, a sealing time of 20 s was used.

3.2. Charge curve Li ‖ LFP

An Arbin LBT21084MC Battery Cycler was used to charge the Li ‖ LFP cell, see Fig. 2. A constant charging current of 0.127 mA was used. The capacity of the cell was 3.76482 mAh at a cell voltage of 4.3 V. The lithium content of $Li_{1-x}FePO_4$ in the figure was estimated from the capacity of the cell, with $x = 0$ at 0 capacity at $x = 1$ at 3.76482 mAh.

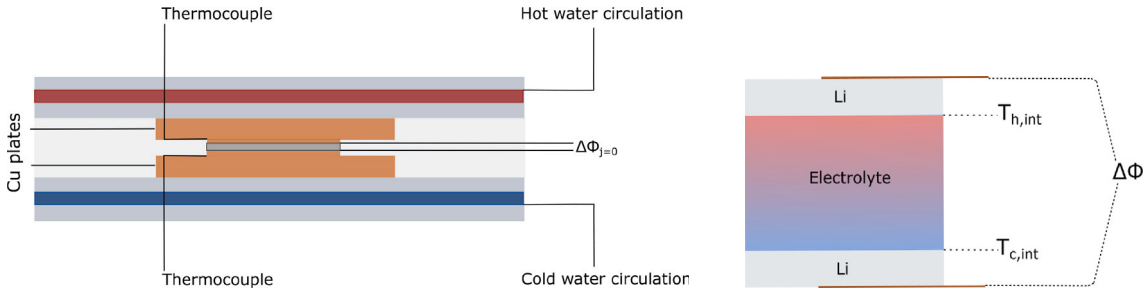

(a) Experimental set-up (b) Shematic of Li-thermogalvanic cell

Fig. 3. Experiment set-up.

3.3. Isothermal reaction entropy measurements

The Li ‖ LFP cell was sandwiched between two copper plates within a frame of two aluminium plates (see Fig. 3(a)). The circulating water was set to the same temperature, and allowed both sides of the cell to be thermostatted. An Agilent 34970A Data acquisition/Switch unit was used to record the electric potential difference between LFP (positive) and Li (negative). Type K thermocouples were placed between the copper plates to measure the temperatures on the two sides. The potential response of the cell was measured when the temperature was changed. Both cells had a negative drift in the potential, indicating self-discharge. All changes in the emf at constant cell temperature came from this drift. A constant drift, calculated from a linear region of the curve, was subtracted when treating the data. Potential curves before and after correcting for the drift are also shown in Fig. 4. The slope of the subtracted drift is stated in the caption of Fig. 4 here and in Figs. 6–21 in the SI.

3.4. Thermogalvanic cell measurements

The same setup as for the reaction entropy measurements were used, but now a temperature difference was applied by circulating water in the aluminium frames (see Fig. 3(a)). The difference was applied by using two water-baths (Grant Ecocool 150R), at different T's. Hot water was circulated in the top plate and cold water in the bottom plate, to avoid convection in the electrolyte. Prior to measurement, the cells were equilibriated by short-circuiting for approximately 30 min. An Agilent 34970 A Data acquisition/Switch unit was used to record the potential difference between the hot electrode (defined as the positive electrode) and the cool electrode (defined as the negative). Afterward short-circuiting, the cells were allowed to reach a stable emf. A bias potential of typically ± 1 mV was recorded prior to and in-between the measurements and subtracted from the reading. The potential response of the cell to an applied temperature difference was measured for up to 16 h. Type K thermocouples were placed between the copper plates to measure the temperatures at the two electrode interfaces.

3.5. Calibration of internal temperature difference

A drawback coming from the choice to assemble the cells as pouch cells is the difficulty in controlling the temperature difference between the electrodes. A control was set-up in a few cases.

In the typical set-up we measured the temperature difference between the Cu plates external to the cell. The temperature difference across the electrodes is needed in the expression for the Seebeck coefficient.

The calibration procedure, to find the last from the first, was therefore set up in the same way as described by Richter [5]. Two type K thermocouples were stripped of insulation and introduced into three Li-symmetric cells in order to record internal temperature differences. These thermocouples were positioned between the cell housing and the metal electrodes. The external temperature difference was controlled and compared to the internal one. The ratio of the two differences were 0.66 ± 0.06 (see Figure 1–3 in the supplementary material). The uncertainty introduced by the calibration was included in the uncertainty of the reported Seebeck coefficients. For LFP, the internal temperature difference was calculated from the difference of the Li-symmetric cells using Fourier's law (see supplementary material).

4. Results

4.1. Reaction entropy of Li ‖ $L_{1-x}FP$

The Li ‖ LFP-cells were characterized by emf values between 2.8–3.4 V. This is within the expected voltage range for this cell when LFP is close to being fully lithiated [21]. The lithium content of our electrodes are within the blue-shaded region in Fig. 2, where small changes in lithium concentration can strongly influence the potential of the electrode.

All cells had a drifting potential. The change in voltage from 3.3/3.4 V to 2.8/3.0 V for cells 1 and 2 respectively, came from a drift that took place over 8 days. Entropy changes are calculated from a corrected potential where the drift from the start to the end of a measurement had been removed. Both cells' drift appeared to be temperature dependent. Because of this, the temperature dependency was difficult to quantify for ΔS measurements with voltages between 3.2–3.3 V for cell 1 and 3.3–3.4 V for cell 2, though qualitatively it was positive and negative respectively (see Figs. 6a and 15 in the supplementary material). For cell 1, this is in agreement with a positive voltage measured for cell 2 between 3.1–3.18 V. At around 3.1 V there was a sign change in the emf response due to a temperature change in cell 1 (see Figure 6b in the supplementary material).

Fig. 4 here, and Figs 6–21 in the supplementary material show temperature dependencies of two Li ‖ LFP isothermal cells, with average values reported in Table 1. Reported voltage curves for $L_{1-x}FP$ show a rapid decrease in the emf when $x \to 0$ [21,23] (cf. Fig. 2), which has been attributed to a phase transition from a two-phase material to a solid solution. The drift might be explained by small changes in lithiation or by a phase transition that occur when LFP is near fully lithiated. We return to this issue in the discussion.

Cell 1 reached a more stable emf temperature dependence between 2.8–2.96 V, with an average slope of −0.66 ± 0.03 mV/K from seven measurements presented in figure 4a–c and figures 8–12 in the SI. The value corresponds to a reaction entropy of −64 ± 3 J/K mol. At 3.25–3.27 V the cell had a positive temperature dependence. It was negative around 3.1 V (see Fig. 6 in Supplementary material). Cell 2 had a negative slope between 3.37–3.4 V. Due to a high self-discharge which appeared to be varying with the temperature, these measurements were used qualitatively only. Similarly to cell 1, cell 2 exhibited a sign change, and had a positive slope of 0.5 ± 0.2 mV/K when the cell voltage was between 3.10–3.18 V, corresponding to a ΔS = 50 ± 20 J/K mol. This value is an average of the measurements

Table 1
Li || $L_{1-x}FP$ entropy differences for cell 1 and 2. The value for Cell 1 is an average of seven measurements, for Cell 2 an average of four measurements. The reported uncertainty is two times the standard error. x-values estimated from nominal capacity. Π^{LFP} are computed from Π^{Li} (see Table 2) and $T\Delta S$ at $T = 298$ K.

Cell	Emf (V)	Estimated x-values	$\partial(\Delta\phi)_{j=0}/\partial T$ (mV/K)	ΔS (J/K mol)	Π^{LFP}_{est} (kJ/mol)
1	2.80–2.96	0-0.0007	−0.66 ± 0.03	−64 ± 3	−13 ± 4
2	3.10–3.18	0.0028–0.0041	0.5 ± 0.2	50 ± 20	−47 ± 9

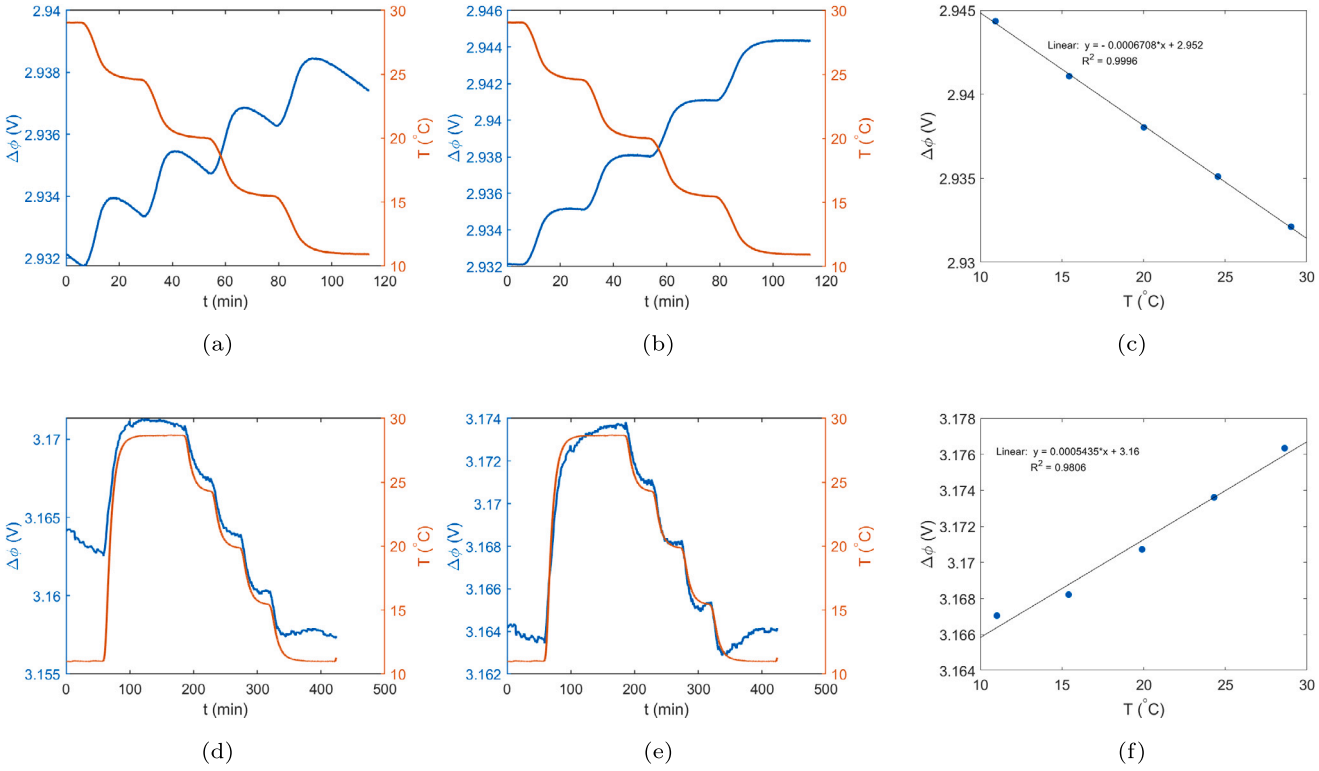

Fig. 4. (a) The emf of Li || LFP cell 1, (b) The emf of Li || LFP cell 1 corrected for a drift of −0.010133 mV/s, (c) The temperature dependency of the emf for cell 1 was found from the slope of a linear regression of the emf against temperature to be −0.67 mV/K in one measurement when the cell emf was around 2.94 V. (d) The emf of Li||LFP cell 2, (e) The emf of Li||LFP cell 2 corrected for a drift of −0.000302 mV/s, (f) The temperature dependency of the emf of cell 2 was found from the slope of a linear regression of the emf against temperature to be 0.54 mV/K in one measurement when the cell emf was around 3.17 V.

shown in figure 4d–e and figures 19–21 in the SI. Note that in these measurements, the potential responded nonlinearly to the temperature change at low temperatures, which is likely to have contributed to the large uncertainty of the computed ΔS. Possible explanations could be that the region is close to where LFP goes through a phase transition, which is temperature dependent, or to a change in the self-discharge with temperature. The point where the temperature reached its set point was chosen for the regression. The potential of the cell at the lowest temperature is most influenced by this, and we see that in all measurements the point contributes to lowering the slope of the regression line.

The entropy measurements document large cell entropy variations for $L_{1-x}FP$ near $x \to 0$.

4.2. Seebeck coefficients and single electrode Peltier heats

Fig. 5 shows typical measurement series of the Seebeck coefficient of Li- and LFP-thermogalvanic cells. The Seebeck coefficients and estimated Peltier heats are given in Table 2.

From Figs. 5(a) and 5(b) here and Figures 20–34 in the supplementary material, we see that Li-thermogalvanic cells quickly reaches a stationary state, typically within one hour. There is no statistically significant difference between the values at initial and stationary state, indicating that the Soret effect is negligible in these cells. We return to this in the discussion. This is not so simple for LFP (see Figs. 35–47 in supplementary material). The LFP cells show differing time-dependent behaviour; some had not reached a stationary state after 16 h.

All cells show a sharp increase as soon as the temperature difference is applied; this is the initial response at uniform conditions. After that, we can roughly divide the time-dependent change into three patterns;

1. The recorded emf quickly reaches a local minimum, followed by a slow increase to a plateau value at stationary state. Cf. Figure 35 in the supplementary material.
2. The recorded emf does not vary much with time, similar to the Li-cells, cf. Figures 39–40 in the supplementary material.
3. The emf curve has a slow increase to a plateau value at stationary state, cf. Figures 37, 41, 43, 44, 45 and 47 in the supplementary material.

In addition we observed that in a few LFP-thermogalvanic cells the shape of the emf-curve changed within a measurement series. We found this to be a reversible and reproducible behaviour, cf. Figs. 5(c) and 5(d) here and Figures 44 and 45 in the supplementary material. We observed that the time-dependency of the emf response changed with ΔT. The sign and magnitude varied, something we would not expect in a bulk electrolyte solution of the same composition.

Neither the lithium-metal cells nor the LFP cells showed significant dependence on the pouch cell sealing procedure. Upon opening the cells, the amount of electrolyte was observed to differ, however. Excess

Table 2
Measured Seebeck coefficients at uniform and stationary state conditions and estimated Peltier heats at 298 K.

Vacuum time (s)	Li			LFP		
	η_0	η_∞ (mV/K)	Π (kJ/mol)	η_0	η_∞ (mV/K)	Π (kJ/mol)
4+4	0.84 ± 0.08	0.81 ± 0.08	−24 ± 2		–	
	1.37 ± 0.13	1.34 ± 0.14	−39 ± 4		–	
6+4	0.93 ± 0.14	0.90 ± 0.09	−27 ± 4		–	
10+4	1.04 ± 0.10	1.01 ± 0.10	−30 ± 3		–	
20+4	0.94 ± 0.09	0.91 ± 0.09	−27 ± 3	0.51 ± 0.05	0.61 ± 0.06	−14.7 ± 1.4
30+4		–		1.8 ± 0.3	2.1 ± 0.3	−52 ± 9
		–		1.9 ± 0.3	1.9 ± 0.3	−55 ± 9
		–		1.6 ± 0.2	1.8 ± 0.2	−46 ± 6
40+4	0.90 ± 0.09	0.84 ± 0.08	−26 ± 3	0.92 ± 0.08	1.0 ± 0.2	−26 ± 2
		–		0.78 ± 0.08	0.75 ± 0.08	−22 ± 2
60+4	1.37 ± 0.13	1.42 ± 0.14	−39 ± 4	2.5 ± 0.3	2.4 ± 0.2	−72 ± 9
	0.83 ± 0.08	0.87 ± 0.08	−24 ± 2	1.7 ± 0.7	1.8 ± 0.5	−50 ± 20
70+4		–		1.6 ± 0.2	2.1 ± 0.2	−46 ± 6
80+4	1.18 ± 0.10	1.23 ± 0.12	−34 ± 3	2.1 ± 0.2	3.5 ± 0.9	−60 ± 6
	1.33 ± 0.13	1.41 ± 0.14	−38 ± 4	2.3 ± 0.3	3.3 ± 0.6	−66 ± 9
		–		1.6 ± 0.3	2.1 ± 0.4	−46 ± 9
99+4	1.13 ± 0.12	1.10 ± 0.11	−32 ± 3	1.2 ± 0.2	1.3 ± 0.1	−35 ± 6
	1.35 ± 0.13	1.43 ± 0.14	−39 ± 4	1.7 ± 0.2	1.8 ± 0.4	−49 ± 6
	1.00 ± 0.10	0.92 ± 0.10	−29 ± 3		–	

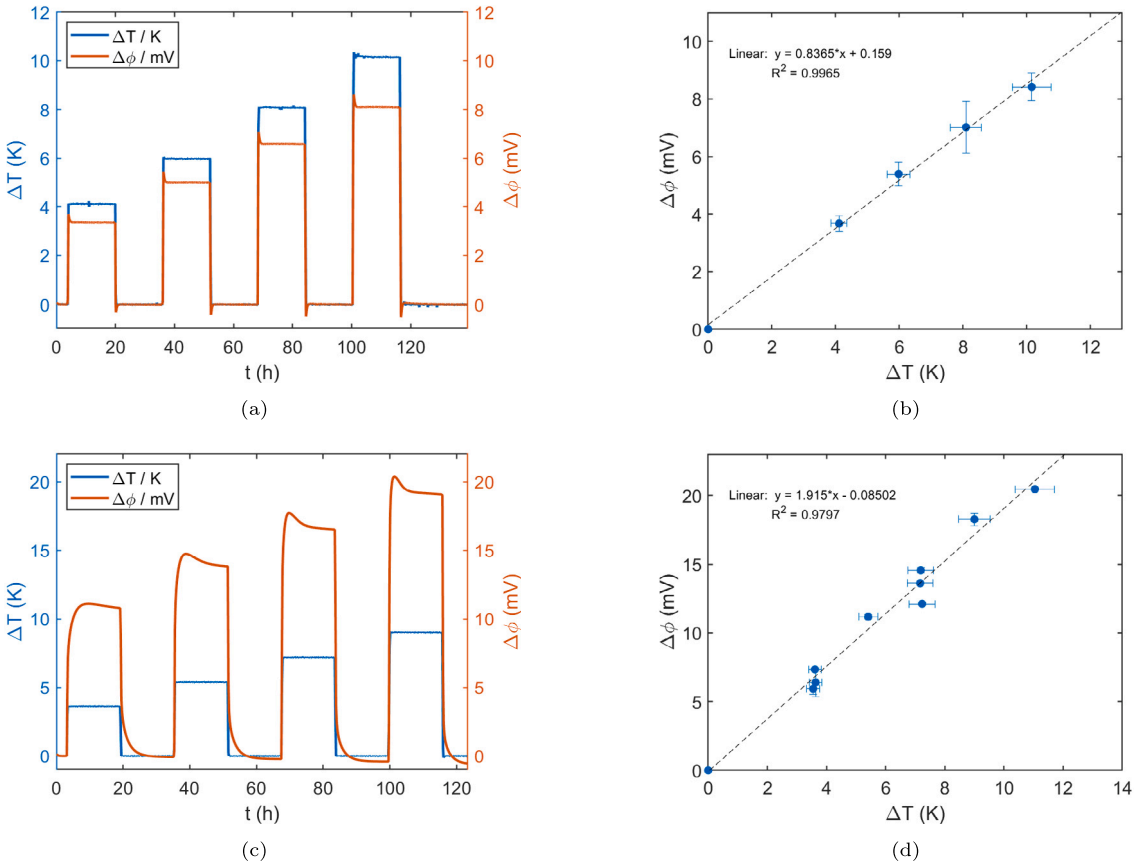

Fig. 5. (a) Emf response to an applied temperature gradient for a Li-thermogalvanic cell with 60 s vacuum sealing. The temperature gradient is the calibrated internal temperature gradient. (b) The Seebeck coefficient is found from linear regression. The error bars represent the uncertainty in the temperature gradient and the uncertainty in the emf response.(c) Emf response to an applied temperature gradient for a LFP-thermogalvanic cell with 30 s vacuum sealing. The temperature gradient is the calibrated internal temperature gradient. (d) The Seebeck coefficient is found from linear regression. The error bars represent the uncertainty in the temperature gradient and the uncertainty in the emf response.

electrolyte is probably more affected by longer sealing procedures and/or evaporation of solvent [39]. Details regarding vacuum-sealing are often not reported, and it has been pointed out that vacuum-sealing may lead to solvent evaporation [40]. Since it appears to be no trend with sealing procedure for either Li nor LFP, we assume that we may neglect variations due to solvent evaporation.

5. Discussion

5.1. Reaction entropy and phase transition of LFP

In this work we have focused on commercial $L_{1-x}FP$ electrodes with $x \approx 0$. The initial emf of the Li ‖ LFP cells were 3.3–3.4 V. The electrodes in the cell entropy measurements had not been cycled. We see from Fig. 2 that the LFP electrodes were close to, but not fully

lithiated, within the region where there is a phase transition to a solid solution. LFP has been observed to chemically delithiate on exposure to air [41]. The electrodes in this study are pristine, but if any lithium loss has occurred prior to cell assembly, the electrode will be left with a slightly lower lithium content.

We have measured large variations in the entropy change of Li ‖ LFP, from −64 ± 3 J/K mol to +50 J/K mol (see Table 1). To the best of our knowledge, no one has reported such large variations in ΔS as reported here for LFP before from emf measurements. We can compare our values to those estimated from Yamada et al.'s work [21] (see Section 1.1.1), who reported heat flow from calorimetric measurements for a Li ‖ LFP cell. From their data, we estimate ΔS between roughly −30 J/K mol and +35 J/K mol for close to fully lithiated states, in the region where LFP is a solid solution. We see a similar trend in our measurement; a negative ΔS towards the highest lithiated states, and a region with a large positive ΔS. Comparing the voltage curves given in their work to that of Fig. 2, we expect that we have used an electrode with a larger particle size in this work.

Large ΔS variations due to phase transitions have also been observed for cobalt oxide electrodes. Reynier and co-workers reported a positive entropy change of +20 J/K mol at an order–disorder transition for Li_xCoO_2 at $x = 0.55$, compared to a negative entropy change of around −20 and −40 J/K mol outside of the phase-transition region [42]. Similar entropy variations for Li_xCoO_2 was also given by Thomas et al.; at x = 0.5–0.75 ΔS values from −60 J/K mol to +30 J/K mol were reported [43].

The potentiometric method to determine reaction entropies assumes a linear relationship in the response of the emf to a temperature change, as can be seen in Eq. (2). However, a non-linear temperature dependence is present in the measurement, as can be seen in Fig. 4d, possibly resulting from a temperature dependent self-discharge. While the temperature step method used in the measurements here are commonly used, other methods have been suggested to minimize the effect of self-discharge and the temperature path on the determination of reaction entropies. Linear temperature ramps [8,44] and alternating positive and negative temperature jumps [45] have been suggested by other groups.

The possibility of a contribution from the Seebeck effect in the leads to the potential giving the entropy was remarked on by Zilberman et al. [45]. In the set-up here, the cell is thermostatted with water circulated in metal frames above and below the cell. If the two metal frames were at different temperatures, this could lead to a thermal gradient across the cell, which would contribute to the measurement. We did not see this in our data.

5.2. Seebeck coefficients and Peltier heats

The results in Table 2 give an average Seebeck coefficient of Li (η_0^{Li}) of 1.1 ± 0.1 mV/K (where the uncertainty is two times the standard error), corresponding to a Peltier heat (Π^{Li}) of −32 ± 3 kJ/mol. This is in agreement with previously reported values between 1.1–1.2 mV/K for 1 M $LiPF_6$ in EC/DMC [16,27], and 1.0–1.6 mV/K for various electrolytes [7,15,28].

For LFP there is no similar average (η_0^{LFP}) value to report; we see a large variation for both the initial and stationary state values. Could these be related to composition changes due to solvent evaporation? If so, we would have expected to see the same for Li-thermogalvanic cells, which we do not. We see from Eq. (9), however, that a variation in ΔS^{LFP}, and hence ΔS, would change the Seebeck coefficient/Peltier heat of LFP.

We have measured large variations in ΔS, including a change in sign, from −64 J/K mol to +50 J/K mol. The variation in reaction entropy supports the observation of large variations in the Seebeck coefficient of LFP. In Table 1 we have used Eq. (1), Π^{Li} = −32 ± 3 kJ/mol and ΔS values in Table 1 to compute Π^{LFP}. From the Peltier heat of LFP, we may also compute η_0^{LFP}. In the region $x = 0 - 0.0007$, we find η^{LFP} = +0.45 ± 0.14 mV/K, in the region $x = 0.0028 - 0.0041$ we compute η^{LFP} = +1.6 ± 0.3 mV/K (note that any error in ΔS from the nonlinear potential response described in Section 4.1 will also be present in this estimate). The measured η_0^{LFP} were between +0.51 ± 0.05 and + 2.5 ± 0.3 mV/K (see Table 2). The observed large variations in reaction entropy can therefore explain a part, if not all of the variations in η_0^{LFP}.

The data support that Eq. (1) can be used to predict Peltier heats in lithium ion battery electrodes. In this work we have used commercial LFP electrodes, with a large electrode particle size. Will the Peltier heat and reaction entropy change, if the particle size is reduced? It is known that LFP electrodes with nanoscale porosities have different phase-transition regions [23]. Are transport properties also affected? More knowledge is needed to establish the impact of the heterogeneous porous nature of the electrodes on the Peltier heat.

We have previously reported that the Seebeck coefficients for LIB electrodes are negative [5,25]; In this study we report only positive Seebeck coefficients, indicating a possible measurement error on our part in earlier publications [5,14,25,29]. A positive value is in agreement with values from other groups [6,7,15,27,28], and measurements done by the group of Schuster [24], who measured the Peltier heat of deposition on lithium-metal electrodes directly.

5.3. Peltier heat vs. entropic heating

We see that the size of the Peltier heat of lithium, −32 ±3 kJ/mol, is larger than $T\Delta S$, which varies from −19 to +15 kJ/mol. The Peltier heat of LFP varies from −15 ± 1, similar in size to $T\Delta S$, to −72 ± 9 kJ/mol, significantly larger. When Li is oxidized (during discharge), 32 kJ/mol is released at the surface, leading to a local temperature rise. At the same time, at lithiated states corresponding to the blue region in Fig. 2, between 15 and 72 kJ/mol is absorbed at the LFP surface as lithium is intercalated, and the electrode cools. The sign switches upon a change in the direction of the current. The net entropic heat in the Li‖LFP cell varies; upon discharge, the cell absorbs heat, i.e. cools, when ΔS is positive, and generate heat when ΔS is negative.

5.4. The time-dependent thermogalvanic potential

A time-dependency of the thermogalvanic potential is usually caused by the Soret effect. Thermodiffusion caused by the Soret effect happens on the same timescale as diffusion. As mentioned in Section 3.1, our system is expected to have a characteristic time between 18–55 min. Due to the porous structure of LFP, we may expect a higher characteristic time for the LFP cells. With measurement times between 4 h (Li-thermogalvanic cells) and 16 h (Li- and LFP thermogalvanic cells), we would expect to be able to observe the Soret effect of the system. We observed a negligible time-dependency of the thermogalvanic potential of the Li-thermogalvanic cells. This could mean that there is a negligible Soret effect in the system. It could also mean that there is mixing in the electrolyte which disturbs the concentration gradients, i.e. convection.

We have seen that the time-dependence of thermogalvanic potential of the LFP cells differs from that of the Li-cells, cf. Figs. 20–47 in the supplementary material. The time-dependent behaviours of the emf of the LFP-thermogalvanic cells are not consistent; the approach to stationary state varies from cell to cell (see figs. 35–47 in the supplementary material). The different time-dependent curves could indicate either (1) that we have different Soret effects in the Li- and LFP cells or (2) that there is another temperature dependent process occurring simultaneously. Both systems contain the same electrolyte; so different curves could be explained by the heterogeneous nature of the porous electrodes, which affects the transport coefficients, cf. Eq. (10).

However, in Fig. 5(c) we also saw a time-dependency in the emf for an LFP-thermogalvanic cell which cannot be explained by Soret

diffusion alone; the curve was temperature gradient dependent, non-symmetric with the relaxation process and the effect was reversible upon removal of the thermal force. We suspect that the effect may be caused by a phase-transition in the heated electrode. The phase transition from a phase separated system to a solid solution is an entropy driven process; and it is promoted at elevated temperatures. In the thermogalvanic cell experiments we heat one electrode and cool the other. A temperature-dependent phase transition would be more favourable for the high T electrode, than the low T electrode.

Another possibility, perhaps more farfetched, is that the presence of a thermal force itself might favour a phase transition. It has been suggested that the thermodynamic driving forces present under normal battery operation suppress the phase separation of LFP and that the electrodes can be in a transient solid solution phase [46]. In other words, it has been suggested that the phase diagram of LFP change during non-equilibrium conditions [47].

We have previously reported large Soret effects that we have been unable to reproduce [5], though the Seebeck coefficients are similar in magnitude to those reported in this work. Perhaps these processes are connected to the phase transition to solid solution. The phase transition can, when shifted along the liquidus line, give rise to reversible thermal effects.

6. Conclusion

We have examined conditions relating the reaction entropy and single electrode Peltier heats in lithium ion batteries with planar and porous electrodes. Our measurements of Peltier heats of lithium-metal of -32 ± 3 kJ/mol agree with previously reported values around -30 kJ/mol. We report large variations in the Peltier heat of $LiFePO_4$, from -15 ± 1 to -72 ± 9 kJ/mol close to full lithiation. The negative sign means that the Li-metal surface generate heat during discharge, while heat is absorbed at as lithium ions are intercalated into LFP. The variations in the Peltier heat of LFP are explained by large measured reaction entropy changes of -64 ± 3 J/K mol to $+ 50 \pm 20$ J/K mol against lithium. The time-dependence of the Seebeck coefficient of the metallic electrode differ from that of the porous electrodes. This indicates that the Soret effects differ from the bulk value in the pores of the electrode.

CRediT authorship contribution statement

Astrid Fagertun Gunnarshaug: Conceptualization, Methodology, Validation, Investigation, Formal analysis, Visualization, Writing – original draft. **Odne Stokke Burheim:** Conceptualization, Methodology, Resources, Supervision, Writing – review & editing, Funding acquisition. **Signe Kjelstrup:** Conceptualization, Methodology, Resources, Supervision, Writing – review & editing, Funding acquisition.

Declaration of competing interest

The authors declare that they have no known competing financial interests or personal relationships that could have appeared to influence the work reported in this paper.

Data availability

Data will be made available on request

Acknowledgements

The authors AFG and SK are grateful to the Norwegian Research Council for their Center of Excellence funding scheme for project no. 262644 PoreLab. OSB is grateful for the financial support from Norwegian University of Science and Technology (NTNU), via the strategic research ENERSENSE (project no. 68024013). Trym Bærheim is acknowledged for his contribution measurement of the charge-curve of the Li || LFP cell.

Appendix A. Supplementary data

Supplementary material related to this article can be found online at https://doi.org/10.1016/j.electacta.2023.142739.

References

[1] T.M. Bandhauer, S. Garimella, T.F. Fuller, A critical review of thermal issues in lithium-ion batteries, J. Electrochem. Soc. 158 (3) (2011) R1.
[2] L. Rao, J. Newman, Heat-generation rate and general energy balance for insertion battery systems, J. Electrochem. Soc. 144 (8) (1997) 2697.
[3] K. Jalkanen, T. Aho, K. Vuorilehto, Entropy change effects on the thermal behavior of a $LiFePO_4$/graphite lithium-ion cell at different states of charge, J. Power Sources 243 (2013) 354–360, http://dx.doi.org/10.1016/j.jpowsour.2013.05.199, URL http://www.sciencedirect.com/science/article/pii/S0378775313010203.
[4] V.V. Viswanathan, D. Choi, D. Wang, W. Xu, S. Towne, R.E. Williford, J.-G. Zhang, J. Liu, Z. Yang, Effect of entropy change of lithium intercalation in cathodes and anodes on Li-ion battery thermal management, J. Power Sources 195 (11) (2010) 3720–3729.
[5] F. Richter, A. Gunnarshaug, O.S. Burheim, P.J. Vie, S. Kjelstrup, Single electrode entropy change for LiCoO2 electrodes, ECS Trans. 80 (10) (2017) 219.
[6] A. Swiderska-Mocek, E. Rudnicka, A. Lewandowski, Temperature coefficients of Li-ion battery single electrode potentials and related entropy changes–revisited, Phys. Chem. Chem. Phys. 21 (4) (2019) 2115–2120.
[7] H. Wang, Y. Zhu, S.C. Kim, A. Pei, Y. Li, D.T. Boyle, H. Wang, Z. Zhang, Y. Ye, W. Huang, et al., Underpotential lithium plating on graphite anodes caused by temperature heterogeneity, Proc. Natl. Acad. Sci. 117 (47) (2020) 29453–29461.
[8] F. Friedrich, S. Pieper, H.A. Gasteiger, Entropy measurements of Li-ion battery cells with Li-and Mn-rich layered transition metal oxides via linear temperature variation, J. Electrochem. Soc. 168 (12) (2021) 120502.
[9] J. Newman, N.P. Balsara, Electrochemical Systems, John Wiley & Sons, 2021.
[10] J. Newman, Thermoelectric effects in electrochemical systems, Ind. Eng. Chem. Res. 34 (10) (1995) 3208–3216.
[11] S. Kjelstrup, D. Bedeaux, Non-Equilibrium Thermodynamics of Heterogeneous Systems, Vol. 20, World Scientific, 2020.
[12] K. Førland, T. Førland, S. Kjelstrup Ratkje, Irreversible Thermodynamics. Theory and Applications, Wiley, Chichester, 1988.
[13] K.E. Thomas, J. Newman, Thermal modeling of porous insertion electrodes, J. Electrochem. Soc. 150 (2) (2003) A176, http://dx.doi.org/10.1149/1.1531194.
[14] A.F. Gunnarshaug, P.J. Vie, S. Kjelstrup, Reversible heat effects in cells relevant for lithium-ion batteries, J. Electrochem. Soc. 168 (5) (2021) 050522.
[15] H. Wang, S.C. Kim, T. Rojas, Y. Zhu, Y. Li, L. Ma, K. Xu, A.T. Ngo, Y. Cui, Correlating li-ion solvation structures and electrode potential temperature coefficients, J. Am. Chem. Soc. 143 (5) (2021) 2264–2271.
[16] Q. Huang, M. Yan, Z. Jiang, Thermal study on single electrodes in lithium-ion battery, J. Power Sources 156 (2) (2006) 541–546.
[17] M. Wang, K. Liu, S. Dutta, D.S. Alessi, J. Rinklebe, Y.S. Ok, D.C. Tsang, Recycling of lithium iron phosphate batteries: Status, technologies, challenges, and prospects, Renew. Sustain. Energy Rev. 163 (2022) 112515, http://dx.doi.org/10.1016/j.rser.2022.112515, URL https://www.sciencedirect.com/science/article/pii/S1364032122004191.
[18] D. Jugović, D. Uskoković, A review of recent developments in the synthesis procedures of lithium iron phosphate powders, J. Power Sources 190 (2) (2009) 538–544, http://dx.doi.org/10.1016/j.jpowsour.2009.01.074, URL https://www.sciencedirect.com/science/article/pii/S0378775309001700.
[19] N.B. Manjong, V. Bach, L. Usai, S. Marinova, O.S. Burheim, M. Finkbeiner, A.H. Strømman, A comparative assessment of value chain criticality of lithium-ion battery cells, Sustain. Mater. Technol. 36 (2023) e00614, http://dx.doi.org/10.1016/j.susmat.2023.e00614, URL https://www.sciencedirect.com/science/article/pii/S2214993723000490.
[20] J.L. Dodd, S. Nishimura, R. Yazami, A. Yamada, B. Fultz, Entropy of lithiation in Li_xFePO4, ECS Meeting Abstracts MA2006-02 (4) (2006) 179, http://dx.doi.org/10.1149/MA2006-02/4/179.
[21] A. Yamada, H. Koizumi, S.-i. Nishimura, N. Sonoyama, R. Kanno, M. Yonemura, T. Nakamura, Y. Kobayashi, Room-temperature miscibility gap in LixFePO4, Nature Mater. 5 (5) (2006) 357–360.
[22] Y. Li, A review of recent research on nonequilibrium solid solution behavior in LiXFePO4, Solid State Ion. 323 (2018) 142–150.
[23] G. Kobayashi, S.-i. Nishimura, M.-S. Park, R. Kanno, M. Yashima, T. Ida, A. Yamada, Isolation of solid solution phases in size-controlled LixFePO4 at room temperature, Adv. Funct. Mater. 19 (3) (2009) 395–403.
[24] M.J. Schmid, K.R. Bickel, P. Novák, R. Schuster, Microcalorimetric measurements of the solvent contribution to the entropy changes upon electrochemical lithium bulk deposition, Angew. Chem., Int. Ed. Engl. 52 (50) (2013) 13233–13237, http://dx.doi.org/10.1002/anie.201305508, arXiv:https://onlinelibrary.wiley.com/doi/pdf/10.1002/anie.201305508, URL https://onlinelibrary.wiley.com/doi/abs/10.1002/anie.201305508.

[25] A.F. Gunnarshaug, S. Kjelstrup, D. Bedeaux, F. Richter, O.S. Burheim, The reversible heat effects at lithium iron phosphate-and graphite electrodes, Electrochim. Acta 337 (2020) 135567.
[26] Y.V. Kuzminskii, V.A. Zasukha, G.Y. Kuzminskaya, Thermoelectric effects in electrochemical systems. Nonconventional thermogalvanic cells, J. Power Sources 52 (2) (1994) 231–242, http://dx.doi.org/10.1016/0378-7753(94)02015-9, URL http://www.sciencedirect.com/science/article/pii/0378775394020159.
[27] N.S. Hudak, G.G. Amatucci, Energy harvesting and storage with lithium-ion thermogalvanic cells, J. Electrochem. Soc. 158 (5) (2011) A572–A579.
[28] J.J. Black, J.B. Harper, L. Aldous, Temperature effect upon the thermoelectrochemical potential generated between lithium metal and lithium ion intercalation electrodes in symmetric and asymmetric battery arrangements, Electrochem. Commun. 86 (2018) 153–156.
[29] A.F. Gunnarshaug, P.J.S. Vie, S. Kjelstrup, Corrigendum: Review—Reversible heat effects in cells relevant for lithium-ion batteries, J. Electrochem. Soc. 170 (4) (2023) 049001.
[30] L. Spitthoff, A.F. Gunnarshaug, D. Bedeaux, O. Burheim, S. Kjelstrup, Peltier effects in lithium-ion battery modeling, J. Chem. Phys. 154 (11) (2021) 114705.
[31] A. Andersson, J.O. Thomas, The source of first-cycle capacity loss in LiFePO4, J. Power Sources 97 (2001) 498–502.
[32] V. Srinivasan, J. Newman, Discharge model for the lithium iron-phosphate electrode, J. Electrochem. Soc. 151 (10) (2004) A1517.
[33] A. Yamada, H. Koizumi, N. Sonoyama, R. Kanno, Phase change in lix FePO4, Electrochem. Solid-State Lett. 8 (8) (2005) A409, http://dx.doi.org/10.1149/1.1945373.
[34] H. Zhou, et al., Two-phase transition of Li-intercalation compounds in Li-ion batteries, Mater. Today 17 (9) (2014) 451–463.
[35] R. von Haase, Thermodynamics of Irreversible Processes, Addison-Wesley, 1969.
[36] J. Landesfeind, H.A. Gasteiger, Temperature and concentration dependence of the ionic transport properties of lithium-ion battery electrolytes, J. Electrochem. Soc. 166 (2019) A3079–A3097.
[37] H. Lundgren, M. Behm, G. Lindbergh, Electrochemical characterization and temperature dependency of mass-transport properties of LiPF6 in EC: DEC, J. Electrochem. Soc. 162 (3) (2015) A413.
[38] L.O. Valøen, J.N. Reimers, Transport properties of LiPF6-based Li-ion battery electrolytes, J. Electrochem. Soc. 152 (5) (2005) A882.
[39] R. Stockhausen, A. Hofmann, L. Gehrlein, T. Bergfeldt, M. Müller, H. Ehrenberg, A. Smith, Quantifying absolute amounts of electrolyte components in lithium-ion cells using HPLC, J. Electrochem. Soc. 168 (8) (2021) 080504.
[40] N.M. Trease, L. Zhou, H.J. Chang, B.Y. Zhu, C.P. Grey, In situ NMR of lithium ion batteries: Bulk susceptibility effects and practical considerations, Solid State Nucl. Magnet. Reson. 42 (2012) 62–70, http://dx.doi.org/10.1016/j.ssnmr.2012.01.004, URL https://www.sciencedirect.com/science/article/pii/S0926204012000185, Solid-State NMR in Materials for Energy Storage and Conversion.
[41] J.F. Martin, A. Yamada, G. Kobayashi, S.-i. Nishimura, R. Kanno, D. Guyomard, N. Dupré, Air exposure effect on LiFePO4, Electrochem. Solid-State Lett. 11 (1) (2007) A12.
[42] Y. Reynier, J. Graetz, T. Swan-Wood, P. Rez, R. Yazami, B. Fultz, Entropy of Li intercalation in Li_xCoO_2, Phys. Rev. B 70 (17) (2004) 174304.
[43] K.E. Thomas, J. Newman, Heats of mixing and of entropy in porous insertion electrodes, J. Power Sources 119–121 (2003) 844–849, http://dx.doi.org/10.1016/S0378-7753(03)00283-0, URL http://www.sciencedirect.com/science/article/pii/S0378775303002830, Selected papers presented at the 11th International Meeting on Lithium Batteries.
[44] T. Liebmann, C. Heubner, M. Schneider, A. Michaelis, Investigations on the reversible heat generation rates of blended Li-insertion electrodes, J. Solid State Electrochem. 23 (2019) 245–250.
[45] I. Zilberman, A. Rheinfeld, A. Jossen, Uncertainties in entropy due to temperature path dependent voltage hysteresis in Li-ion cells, J. Power Sources 395 (2018) 179–184.
[46] Y. Orikasa, T. Maeda, Y. Koyama, H. Murayama, K. Fukuda, H. Tanida, H. Arai, E. Matsubara, Y. Uchimoto, Z. Ogumi, Transient phase change in two phase reaction between LiFePO4 and FePO4 under battery operation, Chem. Mater. 25 (7) (2013) 1032–1039, http://dx.doi.org/10.1021/cm303411t.
[47] P. Bai, D.A. Cogswell, M.Z. Bazant, Suppression of phase separation in LiFePO4 nanoparticles during battery discharge, Nano Lett. 11 (11) (2011) 4890–4896, http://dx.doi.org/10.1021/nl202764f, PMID: 21985573.